Florida Institute of Technology

Scholarship Repository @ Florida Tech

Aerospace, Physics, and Space Science Faculty Publications

Department of Aerospace, Physics, and Space Sciences

7-10-2007

The Mid-Infrared Emission Of M87

Eric S. Perlman

Rachel E. Mason

Christopher C. Packham

Nancy A. Levenson

Moshe Elitzur

See next page for additional authors

Follow this and additional works at: https://repository.fit.edu/apss_faculty

 Part of the Astrophysics and Astronomy Commons

Authors

Eric S. Perlman, Rachel E. Mason, Christopher C. Packham, Nancy A. Levenson, Moshe Elitzur, Justin J. Schaefer, Masatoshi Imanishi, William B. Sparks, and James T. Radomski

The Astrophysical Journal, 663:808–815, 2007 July 10
© 2007. The American Astronomical Society. All rights reserved. Printed in U.S.A.

THE MID-INFRARED EMISSION OF M87

Eric S. Perlman,[1,2] R. E. Mason,[3] Christopher Packham,[4] N. A. Levenson,[5] Moshe Elitzur,[5] Justin J. Schaefer,[4] Masatoshi Imanishi,[6] William B. Sparks,[7] and James Radomski[8]

Received 2006 October 18; accepted 2007 April 9

ABSTRACT

We discuss Subaru and *Spitzer Space Telescope* imaging and spectroscopy of M87 in the mid-infrared (mid-IR) from 5 to 35 μm. These observations allow us to investigate mid-IR emission mechanisms in the core of M87 and to establish that the flaring, variable jet component HST-1 is not a major contributor to the mid-IR flux. The *Spitzer* data include a high signal-to-noise ratio 15–35 μm spectrum of the knot A/B complex in the jet, which is consistent with synchrotron emission. However, a synchrotron model cannot account for the observed *nuclear* spectrum, even when contributions from the jet, necessary due to the degrading of resolution with wavelength, are included. The *Spitzer* data show a clear excess in the spectrum of the nucleus at wavelengths longer than 25 μm, which we model as thermal emission from cool dust at a characteristic temperature of 55 ± 10 K, with an IR luminosity $\sim 10^{39}$ ergs s^{-1}. Given *Spitzer*'s few arcsecond angular resolution, the dust seen in the nuclear spectrum could be located anywhere within $\sim 5''$ (390 pc) of the nucleus. In any case, the ratio of active galactic nucleus (AGN) thermal to bolometric luminosity indicates that M87 does not contain the IR-bright torus that classical unified AGN schemes invoke. However, this result is consistent with theoretical predictions for low-luminosity AGNs.

Subject headings: galaxies: active — galaxies: elliptical and lenticular, cD — galaxies: individual (M87) — galaxies: jets — infrared: galaxies

Online material: color figures

1. INTRODUCTION

M87, the dominant galaxy in the Virgo Cluster, is one of the nearest (distance = 16 Mpc, $1'' = 78$ pc) radio galaxies. Since 1918, when Heber Curtis observed a "curious straight ray" extending from its nucleus, it has been known to host a bright jet that is visible at radio through X-ray wavelengths. The jet, one of the primary hallmarks of M87's nuclear activity, has a complex, knotty structure (see Perlman et al. 2001a [hereafter P01a] and references therein). M87 also exhibits energetic line emission from a disk that is seen to be in Keplerian motion (Ford et al. 1994; Harms et al. 1994). Long-slit spectroscopy of the material within the disk has allowed the mass in the inner 3.5 pc of M87 to be measured at $\approx 3 \times 10^9$ $M_\odot$ (Marconi et al. 1997), implying the presence of one of the most massive known black holes.

M87's proximity allows us to obtain particularly high spatial resolution. Unfortunately, M87 is quite faint in the infrared, with a core flux of only 16 mJy at 10.8 μm (Perlman et al. 2001b, hereafter P01b). This makes *Spitzer* well suited to sensitive observations of the infrared emission from this object, while at the same time the small spatial scales that can be probed make M87 an appropriate mid-infrared (mid-IR) target for the largest ground-based telescopes—albeit one requiring long integrations. The knots in the jet are significantly fainter than the nucleus. Table 1 reviews the locations and extents of major knots in the jet, along with *N*-band fluxes either directly measured or extrapolated from radio/optical data.

Previous ground-based observations showed that most of the mid-IR emission from the core of M87 can be attributed to synchrotron radiation from the innermost regions of the jet (P01b; Whysong & Antonucci 2004), although a minor contribution from dust at $T \lesssim 150$ K could not be ruled out. These results provided strong evidence that the dusty torus of classical unified AGN schemes (Antonucci 1993) may be absent in low-luminosity AGNs. Two recent papers have used *Spitzer* data to address the mid-IR emission processes of M87. Bressan et al. (2006) used 5–20 μm Infrared Spectrograph (IRS) spectra to examine the issue of silicate emission from Virgo Cluster galaxies. They showed that M87, like other Virgo ellipticals, exhibits a silicate emission feature at 10 μm, but that this feature is not spatially resolved by *Spitzer*. Shi et al. (2007) used Infrared Array Camera (IRAC) and Multiband Imaging Photometer for *Spitzer* (MIPS) imaging data to reexamine the origin of M87's mid-IR emission. They found that their photometry of the nucleus plus jet and lobes can be fit by a combination of two synchrotron power laws (usually breaking at optical or higher energies), but that in larger ($1'$) apertures an excess is present over that model. This excess is ascribed to dust in the host galaxy with a luminosity similar to that observed in other brightest cluster galaxies.

In this paper we discuss new mid-IR imaging and spectroscopy of M87 using the Subaru Observatory and *Spitzer Space Telescope*. We combine data from the IRAC, MIPS, and IRS instruments (the latter covering the entire 5–35 μm range) to obtain a more detailed picture of the emission processes in the nucleus and jet. In § 2 we present the observations and data reduction procedures, while in § 3 we discuss M87's line and continuum emission. We close in § 4 with a summary and discussion.

2. OBSERVATIONS AND DATA

2.1. *Ground-based Observations*

Mid-IR imaging and spectroscopy of M87 were obtained on the nights of UT 2005 April 27 and 28 using the Cooled Mid-Infrared

[1] Joint Center for Astrophysics, Physics Department, University of Maryland, Baltimore, MD 21250.
[2] Current address: Department of Physics and Space Sciences, Florida Institute of Technology, Melbourne, FL 32901.
[3] Gemini Observatory, Northern Operations Center, Hilo, HI 96720.
[4] Department of Astronomy, University of Florida, Gainesville, FL 32611.
[5] Department of Physics and Astronomy, University of Kentucky, Lexington, KY 40506-0055.
[6] National Astronomical Observatory, Mitaka, Tokyo 181-8588, Japan.
[7] Space Telescope Science Institute, Baltimore, MD 21218.
[8] Gemini Observatory, Southern Operations Center, La Serena, Chile.

TABLE 1
KNOWN KNOTS IN THE JET OF M87

Knot Name	Distance from Nucleus[a] (arcsec)	Approx. Extent[b] (arcsec)	10.8 μm Flux[c] (mJy)
HST-1[d]	0.8	0.5×0.1	<2.3
D	2.7	1.8×0.2	1.2 ± 0.2
E[e]	6.0	0.9×0.3	0.1
F	8.2	1.4×0.4	1.3 ± 0.2
I[e]	11.2	0.6×0.5	0.25
A	12.4	2.2×1.3	6.4 ± 0.6
B	14.3	2.4×1.3	6.3 ± 0.6
C	17.4	1.9×1.7	4.0 ± 0.6

[a] Location of the flux maximum, rather than centroid.
[b] As measured in optical *HST* images.
[c] Except where noted, as given in P01b.
[d] Knot flux is highly variable; the flux maximum is at the upstream end. The 2 σ flux limit given here is derived from these Subaru data.
[e] Not detected in Gemini images (P01b); fluxes are extrapolated from the radio-optical spectrum (P01a).

Camera and Spectrometer (COMICS) camera (Kataza et al. 2000) attached to the Cassegrain focus of the Subaru Telescope (Iye et al. 2004). The 320×240 SiAs IBC array has a plate scale of $0.129''$ pixel^{-1}, delivering a $41'' \times 31''$ field of view. The detector was read out in correlated quadruple sampling (CQS) mode (Sako et al. 2003). The observing conditions on both nights were not photometric, and the precipitable water vapor was variable, as high as 3–5 mm on April 27, but reaching 5–7 mm on April 28.

For the acquisition images, we used the N11.7 filter (central wavelength 11.67 μm, bandwidth 1.05 μm, 50% cut-on/off). To remove time-variable sky background, telescope thermal noise, and so-called $1/f$ detector noise, we used the standard chop-nod technique, with a $10''$ chop throw at a position angle of -69.5° (measured north through east), to project the jet along the detector rows and place the reference beam between minima in the jet emission. The chop frequency was 0.45 Hz (standard for Subaru COMICS observations), and the total on-source time was 700 s.

We used a similar setup for the spectroscopic observations, with similar chop parameters, but without nodding, as is standard practice with COMICS, and the broad *N*-band order blocking filter. The grating and $0.33''$ slit provided a spectral resolution of $\sim$250 (0.02 μm pixel^{-1}), dispersing the entire *N* band across the array. The superb design and capabilities of COMICS permit on-slit mid-IR imaging of the polished slit jaws, simultaneous with the spectroscopic observations. Thus, we were able to ensure that the emission from the nucleus of M87 passed through the slit and into the spectroscopy arm of COMICS. This proved to be crucial, as differential refraction between the telescope's optical autoguider and the mid-IR science beam moved the object off the slit in as little as 20 minutes at some air masses. The varying, suboptimal conditions meant that M87 was not detected in many of the spectroscopy frames, and only those in which the continuum was visible were stacked and used in the final analysis. The data presented in this paper represent 2100 s of on-source time.

The data were reduced using IRAF and in-house developed IDL routines. The difference for each chopped pair (and for each nod set for imaging) was calculated, and the results were combined until a single frame was created. During the reduction process, chopped pairs obviously compromised by cirrus, high electronic noise, or other problems were discarded.

The point-spread function (PSF) was measured from observations of the photometric standard. The measured full width at half-maximum (FWHM) of the standard was $0.55''$, which agrees well with the FWHM of the spectral trace. Flux calibration was achieved using HD 108985 as a flux standard (Cohen et al. 1992, 1999; Tokunaga 1984) and interpolating the Cohen models to the proper bandpass. Absolute errors in flux calibration were estimated from the variations in the counts through the course of the nights. Given the nonphotometric conditions under which the data were obtained, we estimate an accuracy of at best 15% for the flux calibration.

A 5 pixel extraction aperture was used for the spectroscopy data, and spectral flux calibration was with reference to the telluric standard star, Vega. No attempt was made to correct for slit losses in the spectrum of M87, but we note that the flux density in the calibrated spectrum is comparable to that of both the Subaru COMICS image and the Gemini Observatory Spectrometer and Camera for the Infrared (OSCIR) photometry of P01b. In Figure 1 we show the Subaru image, while in Figure 2 we show the Subaru spectrum.

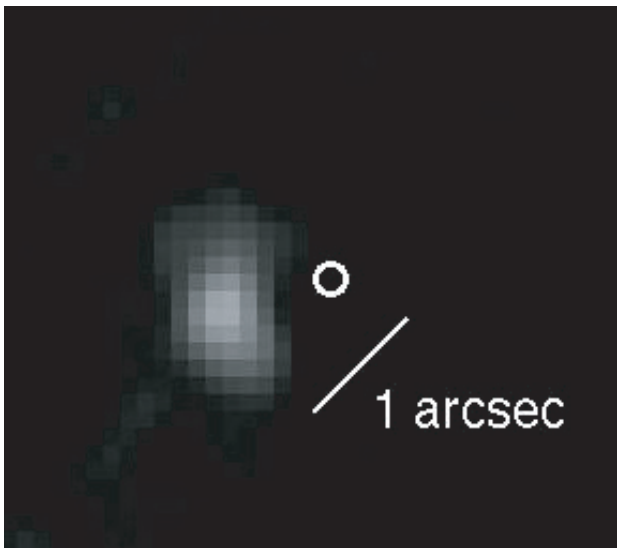

FIG. 1.— Subaru acquisition image of M87. North is up, and east is to the left. The high spatial resolution of the COMICS data is apparent, despite its limited sensitivity. A 3 pixel Gaussian was used to smooth these data. We do not detect emission from knot HST-1, $0.8''$ from the nucleus (location of the circle on this figure). See §§ 2 and 3 for details.

2.2. *Spitzer Observations*

Spitzer Space Telescope observations of M87 were obtained from the *Spitzer* archives. This includes IRS (Houck et al. 2004)

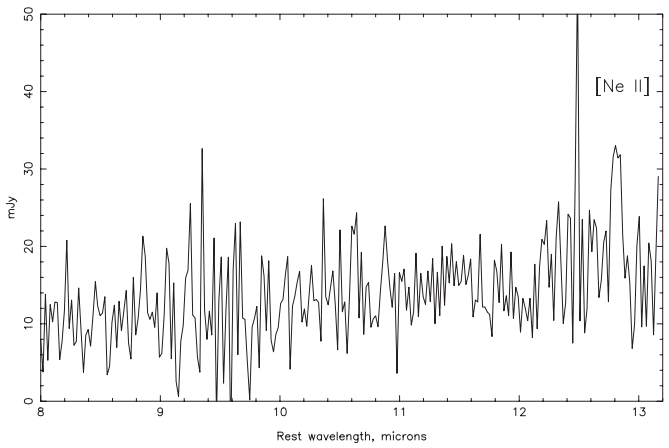

FIG. 2.— Subaru COMICS spectrum of the nucleus, showing the [Ne II] 12.81 μm emission line. See §§ 2 and 3 for details.

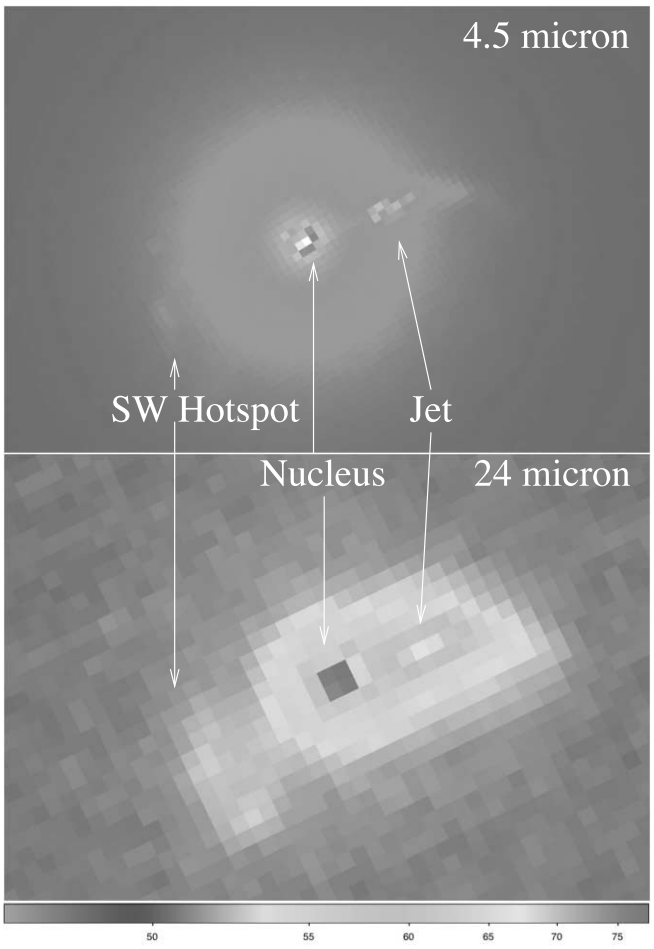

FIG. 3.—*Spitzer* imaging of M87, at 4.5 and 24.5 μm. We have indicated the core, jet, and southwest hot spot for reference. See § 2 for details. [*See the electronic edition of the Journal for a color version of this figure.*]

spectra taken on UT 2004 January 4, as well as MIPS (Rieke et al. 2004) images taken on UT 2004 December 26. Both data sets were acquired as part of PID 82 (PI: Rieke). We also obtained data taken on 2005 June 11 with the IRAC as part of PID 224 (PI: Forman). The advantage of this particular IRS data set is that it covers the full wavelength range of the low-resolution short-wavelength ("short-low") and low-resolution long-wavelength ("long-low") modules. We also comment below on other *Spitzer* data sets.

The IRAC and MIPS data were processed according to the standard pipeline recipes. In both, we used the post–basic calibrated data (post-BCD). Fluxes were extracted using circular apertures appropriate to the diffraction-limited resolution at a given wavelength. Background subtraction was done using annular apertures that included all the flux from the galaxy itself. The *Spitzer* imaging data (shown in Fig. 3) clearly show emission from both the nucleus and the knot A/B complex, as well as extended emission from the galaxy and the southwest hot spot, a feature thought to be associated with the unseen counterjet (Hines et al. 1989; Sparks et al. 1992; Stiavelli et al. 1992). However, individual knots are not resolved at *Spitzer*'s angular resolution ($\approx 3''$ at 10 μm). In this paper, we discuss only the emission from the core and jet knots A and B. We subtracted from the core flux measured on the IRAC data any emission that might be due to galactic emission, using an annulus between $5''$ and $15''$; we also subtracted flux due to the jet by gauging independently the flux in the four quadrants. For this reason our fluxes differ somewhat from those reported in Shi et al. (2007). The 24 μm flux derived in this way agrees fully (within 1σ) with that found in the IRS spectrum of the core (§ 3.1).

The IRS spectra were acquired using both orders of the short-low and long-low modules of the IRS. Total integration times of 28 and 60 s were used for the short- and long-wavelength modules, respectively, and spectra were obtained in two nod positions separated by 1/3 of the slit length, translating into nod throws of $19''$ and $56''$ for the short-low and long-low modules, respectively. The spacecraft roll angle and relative slit position angles were such that the $3.6''$–$3.7''$ wide short-low slits were oriented perpendicular to the jet, while the wider ($10.5''$–$10.7''$) long-low slits were aligned along the jet axis and therefore contain emission from the brightest region of the jet (primarily knots A and B; see Table 1).

After standard pipeline processing, thermal background emission was removed by subtracting spectra taken at the two nod positions, and one-dimensional (1D) spectra then extracted using the *Spitzer* IRS Custom Extractor (SPICE) package. The default extraction apertures ($7.2''$ at 6 μm, $14.4''$ at 12 μm, scaling linearly with wavelength) were employed for the extraction of the short-low data, whereas to better separate the nuclear and jet emission in the long-low data, we used a smaller aperture that varied in size with wavelength, increasing linearly from $5.1''$ at 17 μm to $10.2''$ at 34 μm, comparable to the FWHM of *Spitzer*'s PSF at those wavelengths. As the long-low slits covered both the nucleus and the knot A/B region, we extracted two 1D spectral data sets. No significant fringing is visible in any of the spectra, and no defringing was attempted.

As M87 is an extended source, it is nontrivial to equalize the flux calibration of the orders in both the short-low and long-low modules, or between the two modules, due to the different extraction apertures. As a result, the spectra from different orders may contain differing contributions from the various extended structures, e.g., the various jet components. The nucleus is essentially unaffected by this problem at short wavelengths; however, at longer wavelengths it does have a significant effect. The fact that the nucleus is essentially unresolved at short wavelengths allowed us to use the flux scale from the pipeline for the short-low (SL) data. We then made use of the overlap and "bonus segment" data to match up the flux and slope of the spectral segments blueward and redward of each join. No correction was found to be necessary to scale the SL1 data to that from SL2. However, a scaling factor of 1.67 ± 0.03 was found to be necessary to scale the LL2 data to the SL1 data, while a scaling factor of 1.38 ± 0.03 was necessary to scale the two long-low (LL) orders of the nuclear spectrum.

The knot A/B region, by contrast, is highly extended (about $1.3'' \times 5''$, as measured on the optical and Gemini-N + OSCIR data). This makes the flux calibration process much more complicated, since the SPICE package is not optimized (or intended) to deal with extended sources of this nature. In this case we used the Gemini-N + OSCIR result (P01b) to set the flux scale at 10.8 μm, and then use the best-fit spectral index to extrapolate from the LL spectra down to that wavelength (note that we do not have SL data for the knot A/B region). We then used the overlap and bonus segment data to match up the flux and slope of the spectral segments blueward and redward of the LL1/LL2 join (similarly to what we did for the nucleus). Because the structural details of the knot A/B region are rather different from the nuclear region, a smaller scaling factor (1.04 ± 0.03) was required to scale the LL1 data to the LL2 flux scale once it was fixed using the Gemini-N

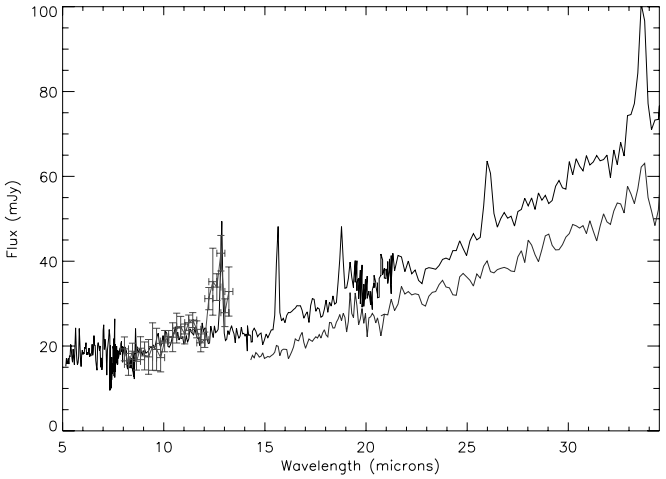

FIG. 4.—*Spitzer* IRS spectrum of the nucleus of M87 (*upper line*) as well as knots A and B (*lower line*). For comparison, the binned Subaru COMICS data are shown in gray (*left*; error bars reflect the standard error on the mean of the points in each bin). To better separate the two IRS spectra, the data for knots A and B have been multiplied by 0.75. Several low-ionization emission lines can be seen in the spectrum of the nucleus, as well as hints of silicate emission around 10 and 18 μm. See §§ 3 and 3.1 for details. [*See the electronic edition of the Journal for a color version of this figure.*]

10.8 μm flux point. The resulting IRS spectra of M87's nucleus and jet are shown in Figure 4.

3. RESULTS

The reduced Subaru acquisition image is shown in Figure 1. The core is clearly detected, with a flux of 20.8 $\pm$ 3.5 mJy, consistent with the findings of P01a to within the 1 σ errors. The error in the flux calibration is dominated by the variable weather conditions. We do not detect any jet features. Even for the knot A/B complex this is not unexpected, given the extended nature of the knot, our short integration time, fairly narrow band, and the poor sky conditions. Surprisingly, however, we do not detect the flaring jet component HST-1 (Harris et al. 2003, 2006; Perlman et al. 2003), 0.8″ from the core, despite the fact that at its peak in 2005 March (just a few weeks before the Subaru observations), its 0.8 μm flux was brighter than that of the core itself (J. A. Biretta et al. 2007, in preparation). We place a limit of 2.3 mJy at 2 σ on the flux from knot HST-1.

The COMICS nuclear spectrum is shown in Figure 2. The signal-to-noise ratio of the spectrum is low, but we detect continuum emission plus a single emission line at 12.81 μm (rest frame). This spectrum contains only flux from the nucleus; the extraction aperture would have excluded any significant contribution from HST-1, which in any case is faint. In Figure 4 we show the *Spitzer* spectrum of the knot A/B region (*lower line*) as well as the nucleus (*upper line*). The signal-to-noise ratio of the *Spitzer* data, while still modest ($\sim$10 pixel^{-1}), is significantly better than that of the Subaru spectrum. We have overplotted on Figure 4 a binned version of the Subaru nuclear spectrum, which matches well with that obtained by *Spitzer*. Despite the difference in angular resolution between the *Spitzer* ($\sim$3″ at 10 μm) and Subaru ($\sim$0.3″) data, the nuclear spectra are similar in flux density and spectral slope in both data sets. This confirms that HST-1 (which in the *Spitzer* data would not be resolved from the nucleus) makes no more than a minimal contribution to the nuclear spectrum. Both the noise in the Subaru data, however, and the known optical variability of the nucleus and HST-1 (measured to be as large as 50% and 500%, respectively; Tsvetanov et al. 1998; Perlman et al. 2003) prevent us from setting stricter limits on the mid-IR flux of HST-1.

The overall similarity of the spectral shapes of the nucleus and the knot A/B complex, at least below 25 μm, confirms the synchrotron nature of the majority of the nuclear emission, first shown by P01b. A close examination of the nuclear and jet spectra does, however, reveal differences. The first of these is the presence of five obvious emission lines in the spectrum of the nucleus, whereas only one weak emission line is seen in the knot A/B spectrum. A more subtle difference is that the nuclear spectrum contains a sharper upturn toward longer wavelengths. We discuss the spectral data in more depth in §§ 3.1–3.2. Note that in the discussion that follows, we use the terms "nuclear region" and "nuclear spectrum" to refer to the *Spitzer* spectrum taken at the position of the nucleus (as opposed to that of the knot A/B region), while what we term as the core refers only to the regions within $\sim$0.3″ of the central black hole (and thus unresolvable in ground-based *N*-band images).

3.1. *Infrared Continuum Emission*

The IR continuum of a galaxy can contain emission from a number of different components. In the case of M87, the most likely sources are thermal emission from warm or cool dust, synchrotron emission from the jet, and (at shorter wavelengths) starlight from K and M stars. In order to determine the nature and origin of this IR emission, it is necessary to correctly account for all possible sources that could fall within the slit and beam of *Spitzer* at any given wavelength. At *Spitzer*'s angular resolution the nuclear spectrum will contain a contribution from emission in the jet (and vice versa; see Table 1), and, because of the decrease in spatial resolution toward longer wavelengths, the magnitude of that contribution will increase with wavelength. We have modeled both the nuclear and knot A/B spectra, and accounted for this effect as follows.

We model each component as a 1D Gaussian of width equal to *Spitzer*'s diffraction limit (which we take to be a Gaussian of FWHM 2.96″ at 10 μm, located at its flux maximum position [Table 1]). We then integrate each Gaussian across the slit (see § 2.2 for details). We use the fluxes of jet knots C, D, and F of P01b, and take their positions and radio-optical spectral indices $\alpha_{\rm RO}$ from P01a ($F_\nu \propto \nu^{-\alpha}$). For fainter knots, we take 2.1 μm fluxes and positions from P01a and extrapolate to 10 μm using the $\alpha_{\rm RO}$ values in P01a. For knots A and B, we fix the fluxes to be equal to those observed by P01b but allow their spectral index to vary. We do not include a contribution from HST-1, given that we do not detect it in our 11.7 μm image (but see below). The modeling of the knot A/B region spectrum is shown in Figure 5. We show separate curves for the contributions of the core, knot A/B, and other knots to the observed spectrum. This modeling procedure can satisfactorily account for the observed spectrum of the knot A/B region. We fit a power law to the spectrum of the knot A/B emission by holding constant the contributions from all other components to the fluxes and spectral indices from P01a and P01b, with the exception of the core (for which we used the power-law fit we detail below). Once this is done, we obtain a best-fit spectral index for knots A and B of $\alpha_{\rm IR} = 0.75 \pm 0.04$. This is within 1 σ of the radio-optical spectral indices given in P01a for these knots. Thus, the spectrum of the knot A/B region is entirely consistent with synchrotron emission, as previously modeled by P01a, P01b, and Shi et al. (2007).

In Figures 6 and 7 we show the modeling of the nuclear spectrum, with Figure 6 showing the 5–35 μm region alone and Figure 7 extending it to longer wavelengths. To fit the nuclear spectrum, we need to add to the jet components an increase of

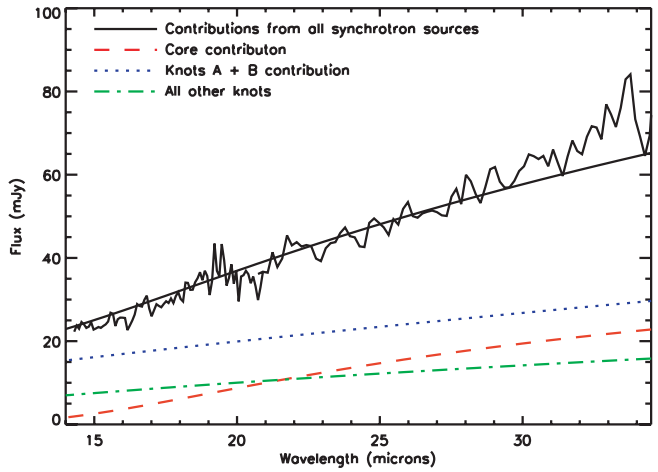

FIG. 5.—*Spitzer* IRS spectrum of jet knots A and B, modeled as discussed in § 3.2. In blue, we show the contribution due to knots A and B (summed); in red, we show the contribution from the core, and in green the contribution from all other knots. The black line represents the sum of the contributions from the core and all knots. The observed spectrum for knots A and B can be satisfactorily reproduced with these synchrotron components.

flux of 15% over that observed at 10.8 μm by P01b. Significant nuclear variability in M87 has previously been noted in the optical by Tsvetanov et al. (1998) and Perlman et al. (2003). In addition, our data require a core spectral index that is quite different from that predicted by P01b, specifically $\alpha_{\rm IR} = 0.41 \pm 0.05$ instead of $\alpha \sim 1.0$ (as used also in other papers, including Shi et al. 2007). This indicates a synchrotron peak frequency $\gtrsim 5 \times 10^{13}$ Hz (and likely $>10^{14}$ Hz), at least 1–2 decades higher in frequency than that fit by P01b. The spectral index was fit only over the spectral range 7.5–15 μm where no departure is observed from a pure power-law form (see below), but the method was otherwise identical to the one above for the knot A/B spectrum. The different spectral index could be the result of variability, as in blazars (of which M87 is a somewhat misaligned example), where increases in flux are often accompanied by spectral hardenings and large increases in peak frequency (see, e.g., Pian et al. 1998). As already noted, the nucleus of M87 is known to be variable in the optical (Tsvetanov et al. 1998; Perlman et al. 2003) on timescales of $\sim$1 month, and on even shorter timescales in the gamma rays (Aharonian et al. 2006).

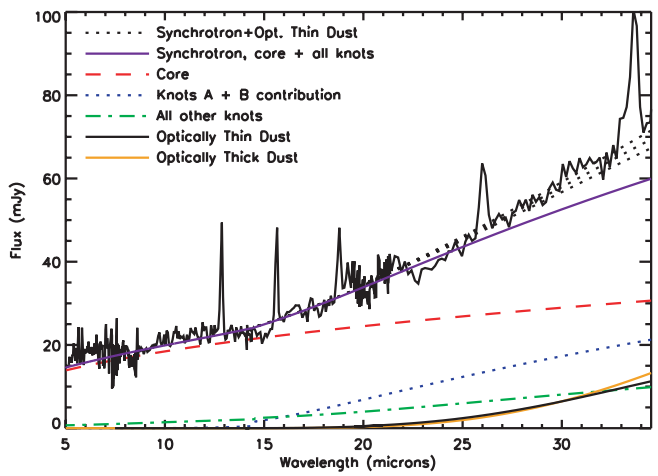

FIG. 6.—*Spitzer* IRS spectrum of the nucleus of M87, modeled as discussed in § 3.1. We follow Fig. 5 by showing the contributions of the core and the knot A/B region as red and blue, respectively, while in green we show the contribution from all other knots. This figure shows the sum of these components as purple, and then optically thin and thick thermal dust emission models as the lower black and orange curves, respectively. The top set of black curves represents the sum of all synchrotron emission plus the optically thin dust model. The upper and lower black dotted curves represent the result of multiplying the 55 K thermal model by 1.2 and 0.8, respectively; this illustrates the range of normalizations to which the data are sensitive.

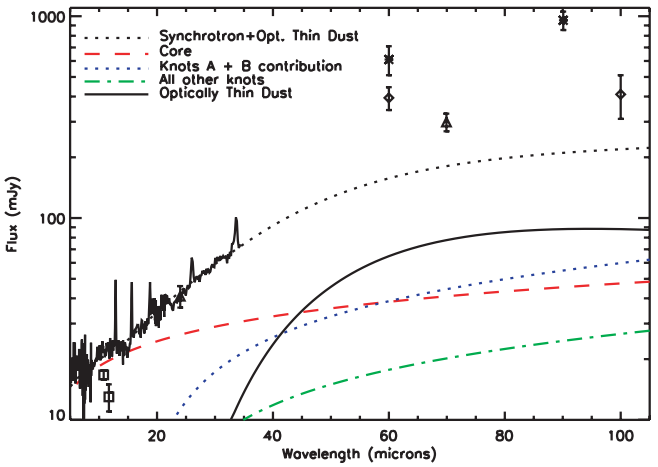

FIG. 7.—*Spitzer* IRS spectrum and models of the nucleus of M87, here plotted with a logarithmic y-axis and the wavelength axis continued up to 105 μm. All curves are the same as in Fig. 6, with the exception of the optically thin thermal emission component, shown in the solid black line (optically thick thermal emission models are not shown). Note that longward of 45 μm, thermal emission becomes dominant, a situation that continues to be the case up to much longer wavelengths. Individual points are shown representing data from *Spitzer* MIPS (*triangle*), *IRAS* (*diamonds*), and *ISO* (*asterisks*). Also shown (*squares*) are flux points from P01b and Whysong & Antonucci (2004), which most likely lie below our data because of variability. We do not attempt to fit data at longer wavelengths; however, if all the dust were at $T < 45$ K, it would overpredict the *IRAS* and *Spitzer* MIPS 70 and 160 μm fluxes.

In contrast to the knot A/B spectrum, we cannot model the observed nuclear emission with the purely power-law emission characteristic of synchrotron radiation. The pure power-law model has discrepancies both at the short-wavelength and long-wavelength end of the IRS spectrum. There are two likely causes of the apparent short-wavelength excess. The first possibility is that it is due to M and K stars in the nuclear regions of M87, a component that P01b speculated might account for the faint (7% of nuclear flux), extended emission found in the much deeper OSCIR image. A second possibility is that the excess might be the low-frequency tail of the emission from knot HST-1, which *Spitzer* would be unable to resolve from the nucleus itself. If we were to use a power law to extrapolate the observed excess at $\sim$5 μm down to a wavelength of 0.8 μm, the flux from this additional component would equal or slightly exceed that of the core, consistent with the observed 0.8 μm flux of knot HST-1 in 2005 January (J. A. Biretta et al. 2007, in preparation).

At longer wavelengths, beyond about 23 μm, we see a much more pronounced excess (Fig. 6). By 35 μm the pure synchrotron model—which includes emission from the core plus all jet knots (i.e., all known sources of synchrotron emission in M87)—underestimates the observed nuclear spectrum by about 20%. This excess could be fit by adding an additional power-law component with spectral index $\alpha_{\rm excess} \sim 6$. However, such a component would be unphysical, given known models of synchrotron radiation (e.g., Leahy 1991); and moreover, our model has already accounted for all known sources of synchrotron emission. Also, the addition of such a steep power-law component would dominate over all the other emission sources by $\sim$50 μm, producing a huge excess by 100 μm, something that is ruled out by the longer

wavelength MIPS and *IRAS* data (Fig. 7).[9] Alternatively, we can fit this excess with thermal emission (Fig. 6), which is not unexpected in the nuclear regions of M87, given the dust lanes found in *Hubble Space Telescope* (*HST*) and ground-based images (e.g., Sparks et al. 1993; Ford et al. 1994). We believe that thermal emission from cool dust in the nucleus is the most physically realistic explanation for the long-wavelength excess in the few arcsecond aperture IRS data (distinct from the host galaxy dust detected at large radii by Shi et al. [2007] in 1′ aperture photometry). In addition, the data and modeling presented here allow us to place constraints on the mass and temperature of dust in the nucleus of M87.

A single blackbody fit to this component yields adequate fits with temperatures between 45 and 65 K, with higher temperatures being unable to reproduce the rise at 23–35 μm, and lower temperatures resulting in an overproduction of the long-wavelength fluxes from *IRAS* and *Spitzer*. We are unable to constrain whether the dust is optically thin or thick (both curves are shown in Fig. 6, for a characteristic temperature of 55 K); however, given that the dust filaments in the nuclear regions of M87 are also typically marked by Hα emission (Sparks et al. 1993; Ford et al. 1994), and also given the low X-ray absorbing column (Perlman & Wilson 2005) the optically thin model may be more likely to be correct.

Figure 7 shows only a 55 K thermal component, as does Figure 6. Although temperatures as low as 45 K are compatible with the data, and in fact a single 45 K thermal emission component can account for all the IRS, MIPS, and *IRAS* data, a single dust temperature this low would mean that the dust in the innermost 5″ of the galaxy contributes much more flux than dust at radii between 5″ and 20″. As M87 is extended at mid-IR wavelengths (e.g., Fig. 3), we consider this unlikely. However, sensitive, higher angular resolution observations at 30–100 μm would be required to put tighter constraints on dust temperatures and optical thicknesses in the nucleus of M87.

The total luminosity of the thermal component revealed by the *Spitzer* spectra is, for $T = 55$ K, 9.7×10^{38} ergs s (2.6×10^5 $L_\odot$). This figure is highly temperature dependent—for $T = 45$ K we find a thermal luminosity of 3.1×10^{39} ergs s, while for $T = 65$ K, we find a thermal luminosity of 2.9×10^{38} ergs s. (By comparison, the error in the normalization of the thermal component, indicated on Fig. 6, is significantly smaller, approximately 20%.) Thermal radiation from dust is therefore a significant contributor to M87's IR emission, being 20%–150% as bright as the core's synchrotron emission between 1 and 300 μm. It is interesting to consider how much dust could account for this thermal emission, and where the dust would be located. If the dust is heated entirely by the AGN, it must be within a few parsecs of the core. If it is at larger distances, it would have to be heated by other mechanisms, for instance, within the star-forming disk tentatively detected by Tan & Blackman (2005). Using standard formulae (Draine 2003 and references therein) and assuming an optically thin dust component, we derive a dust mass of 83 $M_\odot$ for a temperature of $T = 55$ K. This figure is similarly temperature dependent: for $T = 45$ K we find a dust mass of 180 $M_\odot$, while for $T = 65$ K we find a dust mass of 19 $M_\odot$. This is a tiny mass compared to that found in the dusty Hα filaments that extend throughout the galaxy (Sparks et al. 1993.

3.2. *Spectral Features*

The 5–35 μm spectral region covers a range of dust and molecular emission and absorption features, as well as many fine-structure lines. As mentioned above, a line at 12.8 μm is detected in the COMICS spectrum of M87. We ascribe this feature to [Ne II] rather than the 12.7 μm PAH band because of the lack of other molecular features (including the stronger 11.2 μm PAH feature) in both the COMICS and IRS spectra. In addition, the IRS spectrum of the nucleus (Figs. 4 and 6) also contains lines of [Ne III] 15.6 μm, [S III] 18.7 μm, [O IV] + [Fe II] 25.9 μm, and [S III] 33.5 μm, while in the knot A/B spectrum (Figs. 4 and 5), we detect only one emission line at low significance, namely [S III] 33.5 μm. (The [Ar II] 7.0 μm line in the spectrum of Bressan et al. [2006] is not clearly detected in our lower signal-to-noise ratio spectrum.) Table 2 shows the fluxes of the detected lines in the nuclear spectrum, obtained by direct integration under each line and using a continuum level determined by the mean of several points at either side.

TABLE 2
FLUXES OF THE FINE-STRUCTURE LINES DETECTED IN M87

Line, λ_{rest}[a] (μm)	Flux (10^{-21} W cm^{-2})	E_{ion}[a] (eV)
[Ne II] 12.81	1.9[b]	21.6
	5.4[c]	21.6
[Ne III] 15.56	4.1	41.0
[S III] 18.71	2.0	23.3
[O IV]/[Fe II] 25.89/25.99	1.9	54.9/7.9
[S III] 33.48	4.5[d]	23.3

[a] From Sturm et al. (2002).
[b] Subaru COMICS data.
[c] *Spitzer* IRS data.
[d] See text for discussion.

With the exception of [O IV], which may in principle contribute to the 25.9 μm line, the ionization energies of all of the lines are low enough (<50 eV) that they can be excited by massive stars and ionizing shocks. High-excitation lines such as [Ne V] 24.3 μm, which can be strong in AGNs (e.g., Sturm et al. 2002), are not observed in the spectrum of M87. Comparison of line fluxes in different apertures suggest that the line-emitting region may be extended. For instance, the [Ne II] line in the COMICS spectrum is a factor of about 3 weaker than the same line in the larger aperture *Spitzer* spectrum. Although the continuum level for the [Ne II] line in the COMICS spectrum cannot be determined with great accuracy, such a pronounced difference implies that the line-emitting material extends beyond the compact central source observed with COMICS. This interpretation is supported by the fact that we observe a factor of about 2.5 lower flux in the [O IV]/[Fe II] line than in the [Fe II] line in a $14'' \times 20''$ aperture *Infrared Space Observatory* (*ISO*) spectrum of M87 (Sturm et al. 2002). The *ISO* spectrum had sufficient spectral resolution to separate the [O IV] 25.89 μm and [Fe II] 25.99 μm lines, but no lines other than [Fe II] were detected. As expected, all the lines are unresolved in the $R \sim 100$ IRS spectrum.

The lack of high-excitation lines is consistent with the classification of M87's nucleus as a LINER (a suggestion originally made by Willner et al. 1985). This might be considered surprising, given the luminosity of M87's jet. However, recent radio observations suggest that relativistic jets may be quite common among LINERs (Nagar et al. 2000; Falcke et al. 2000; Filho et al. 2004). Moreover, due to relativistic beaming, only a very small solid angle of the emission-line regions would be exposed to significant high-energy radiation from the jet.

The [S III] 33.5 μm seen weakly in the knot A/B spectrum (Figs. 4 and 5) is unlikely to come from knots A and B, since spectra of M87's jet have been taken many times in other bands, most

[9] Note that the *ISO* 60 and 100 μm fluxes (Haas et al. 2005) are more than a factor of 2 above all other photometry at similar wavelengths.

recently by *HST* in the UV (Gelderman & Woodgate 1999), and have failed to detect line emission, placing severe limits on the presence of nonstripped nuclei entrained within the jet. It is possible that the [S III] emission originates in the Hα filaments within a few arcseconds of the knot A/B complex (see Sparks et al. 1993). Alternatively, the emission may originate from material close to the nucleus, whose light contributes to the jet spectrum particularly at longer wavelengths where the PSF is largest. This is consistent with the relative contribution of the core to the knot A/B spectrum at 33.5 μm, as computed in our modeling procedure (§ 3.1). That only [S III] 33.5 μm, the longest wavelength line in the nuclear spectrum, is also observed in the jet spectrum suggests that this may be the more likely explanation.

In highly obscured objects, such as Seyfert 2 galaxies, the AGN unified model predicts absorption features near 10 and 18 μm due to the Si—O bond stretch in silicate dust grains. Such features are indeed observed quite widely in Seyfert 2 galaxies (e.g., Roche et al. 1991). Such a feature would not necessarily be expected in M87, however, due to the fact that its jet (which would be perpendicular to any dusty torus under unified schemes) is seen at a fairly small angle to the line of sight ($\lesssim 15^\circ$–20°; Biretta et al. 1999). Consideration of the difference between means in points at the peak and either side of a typical silicate absorption profile in the COMICS spectrum allows us to put a 95% confidence limit of $\tau(9.7) \lesssim 0.34$ on any broad silicate absorption feature in the nucleus of M87. Thus, while a strong absorption feature can be ruled out, this limit is comparable to the silicate optical depth observed in the circumnuclear material of Seyfert 2 galaxies such as NGC 1068 ($\sim$0.4; Roche et al. 1984; Jaffe et al. 2004; Mason et al. 2006). It is also consistent with the best available limit ($N_{\rm H} < 6 \times 10^{20}$ cm^{-2}; much lower than that seen in typical Seyfert 2 galaxies) on nuclear absorption from *Chandra* X-ray data (Perlman & Wilson 2005), given the recently found correlation between X-ray N(H) figures and silicate absorption (Shi et al. 2006).

While the COMICS spectrum sets weak limits on the presence of a 9.7 μm absorption band in the central $<0.65''$ of M87, the IRS spectrum can be used to search for dust features that may exist on somewhat larger scales. In fact, there are hints of weak silicate *emission* features around 10 and 18 μm in the IRS spectrum (the 10 μm feature would be well within the noise of the COMICS spectrum). The 10 μm emission feature is also evident in the IRS spectrum of M87 presented by Bressan et al. (2006; their spectrum does not cover wavelengths >20 μm). Previously thought to be rare in AGNs, silicate emission features have now been seen in the LINER NGC 3998 (Sturm et al. 2005) as well as in several distant quasars (e.g., Hao et al. 2005; Siebenmorgen et al. 2005). Although the AGN unified scheme in its most basic form predicts a silicate emission feature from the hot inner edge of a dusty circumnuclear torus, the apertures so far used to detect the silicate feature do not place strong constraints on the location of the silicate-emitting material in these galaxies. Furthermore, the cool ($\sim$200 K) temperature implied by the strengths and profiles of the features in the LINER, NGC 3998, suggests an origin in narrow-line region dust rather than the inner regions of the torus (Sturm et al. 2005). Although Bressan et al. point out that the 10 μm feature in their data is not spatially extended, the PSF of *Spitzer* at 10 μm ($3''$) is several times larger than the FWHM of the nucleus itself in higher resolution ground-based data. Therefore, it is entirely possible that the silicate emission could be produced by dust as far as 200 pc from the nucleus. *HST* and ground-based optical observations show the existence of a significant amount of warm dust in the inner $3''$ of M87, as evidenced by the Hα emission in many of these regions (Sparks et al. 1993; Ford et al. 1994). Therefore, the silicate emission in M87 does not necessarily imply the existence of a nuclear torus.

4. SUMMARY AND CONCLUSIONS

We have presented mid-IR imaging and spectroscopy of M87, using the Subaru Observatory and the *Spitzer Space Telescope*. The *Spitzer* spectroscopy covered both the nucleus and the knot A/B complex in the jet. The knot A/B spectrum can be well modeled by power-law spectra, as expected for synchrotron emission from jet components, with mid-IR fluxes consistent with those published by P01b and spectral indices consistent with the optical-radio spectra of P01a. However, the *Spitzer* spectrum of the nucleus cannot be modeled by power-law synchrotron emission from the core plus components in the jet. We see clear signs of an IR excess in the core, which can be well modeled by a thermal spectrum with a characteristic temperature of 55 ± 10 K. The low temperature and luminosity of this component (§ 3.2) are consistent with the limits found by P01b.

Whysong & Antonucci (2004) made a similar argument based on 11.7 μm photometry. The present data support and enhance this result, as the thermal contribution is isolated and measured separately from the synchrotron contribution. The measured luminosity is an upper limit to the amount of emission from a dusty torus in M87; the thermal contribution measured in the $10.7''$ wide IRS slit could arise anywhere within 420 pc of the nucleus and need not be associated with a torus at all. Moreover, given that the bolometric luminosity of M87 is $\sim 10^{42}$ ergs s^{-1} (e.g., Reynolds et al. 1996), classical torus models would predict a mid-IR luminosity at least that high (e.g., Risaliti & Elvis 2004). By comparison we observe a much smaller thermal IR luminosity ($\sim 10^{39}$ ergs s^{-1}), making our observations difficult to reconcile with standard unified models of AGNs.

What is the overall significance of the weakness of the torus emission in M87, both for this galaxy and for FR I radio galaxies as a whole? One strong possibility is that the weakly emitting or absent torus in M87 may be a consequence of the AGN's low luminosity. In the disk wind scenario, optically thick regions of an outflowing wind comprise the geometrically and optically thick "torus." In the model of Elitzur & Shlosman (2006), the torus disappears at low luminosities ($\lesssim 10^{42}$ ergs s^{-1}), because accretion onto the central black hole can no longer sustain the large-scale outflows. That we do not detect the mid-IR signature of the classical torus is entirely consistent with the predictions of the disk wind model. An alternative to the disk wind scenario was offered by Reynolds et al. (1996) and di Matteo et al. (2003), who modeled the nucleus of M87 with advection-dominated accretion flow (ADAF) models. Both of those papers derive accretion rates as much as 4 orders of magnitude below the Eddington rate, which di Matteo et al. speculate may signal that M87's nuclear activity is at a very late evolutionary stage. It is important to note, however, that ADAF models do not in and of themselves incorporate the notion of a torus. Finally, it is important to point out that the lack of significant torus emission in M87 does not yet constitute strong evidence that FR Is, as a class, lack luminous tori, although *Spitzer* observations indicate that a significant number may lack this component (Ogle et al. 2006; M. Birkinshaw et al. 2007, in preparation). Cen A, for example, shows significant thermal dust emission in the mid-IR, on scales ranging from the unresolved subparsec scale (likely the torus) to much larger scale emission (Whysong & Antonucci 2004; Hardcastle et al. 2006; Radomski et al. 2007).

Based in part on data collected at Subaru Telescope, which is operated by the National Astronomical Observatory of Japan. We

wish to thank the Subaru Time Allocation Committee (TAC) for their support and the Subaru staff, particularly T. Fujiyoshi, M. Lemmen, and M. Letawsky, for supporting our observations. E. S. P. acknowledges support from NASA LTSA grants NAG5-9997 and NNG05-GD63G, as well as *HST* grant GO-9705. C. P. acknowledges support from NSF grant 0206617. N. A. L. acknowledges work supported by the NSF under grant 0237291. M. E. acknowledges support from NSF grant 0507421 and NASA grant NNG05-GC38G. R. M. and J. R. were supported by the Gemini Observatory, which is operated by the Association of Universities for Research in Astronomy, Inc., on behalf of the international Gemini partnership of Argentina, Australia, Brazil, Canada, Chile, the United Kingdom, and the United States of America. M. I. is supported by Grants-in-Aid for Scientific Research (16740117).

REFERENCES

Aharonian, F., et al. 2006, Science, 314, 1424
Antonucci, R. R. J. 1993, ARA&A, 31, 473
Biretta, J. A., Sparks, W. B., & Macchetto, F. D. 1999, ApJ, 520, 621
Bressan, A., et al. 2006, ApJ, 639, L55
Cohen, M., Walker, R. G., Barlow, M. J., & Deacon, J. R. 1992, AJ, 104, 1650
Cohen, M., Walker, R. G., Carter, B., Hammersley, P., Kidger, M., & Noguchi, K. 1999, AJ, 117, 1864
di Matteo, T., Allen, S. W., Fabian, A. C., Wilson, A. S., & Young, A. J. 2003, ApJ, 582, 133
Draine, B. T. 2003, ARA&A, 41, 241
Elitzur, M., & Shlosman, I. 2006, ApJ, 648, L101
Falcke, H., Nagar, N. M., Wilson, A. S., & Ulvestad, J. S. 2000, ApJ, 542, 197
Filho, M. E., Fraternali, F., Markoff, S., Nagar, N. M., Barthel, P. D., Ho, L. C., & Yuan, F. 2004, A&A, 418, 429
Ford, H. C., et al. 1994, ApJ, 435, L27
Gelderman, R., & Woodgate, B. E. 1999, BAAS, 194, 4905
Haas, M., et al. 2005, A&A, 442, L39
Hao, L., et al. 2005, ApJ, 625, L75
Hardcastle, M. J., Kraft, R. P., & Worrall, D. M. 2006, MNRAS, 368, L15
Harms, R. J., et al. 1994, ApJ, 435, L35
Harris, D. E., Biretta, J. A., Junor, W., Perlman, E. S., Sparks, W. B., & Wilson, A. S. 2003, ApJ, 586, L41
Harris, D. E., Cheung, C. C., Biretta, J. A., Sparks, W. B., Junor, W., Perlman, E. S., & Wilson, A. S. 2006, ApJ, 640, 211
Hines, D. C., Owen, F. N., & Eilek, J. A. 1989, ApJ, 347, 713
Houck, J. R., et al. 2004, ApJS, 154, 18
Iye, M., et al. 2004, PASJ, 56, 381
Jaffe, W., et al. 2004, Nature, 429, 47
Kataza, H., Okamoto, Y., Takubo, S., Sako, S., Nakamura, K., Miyata, T., & Yamashita, T. 2000, Proc. SPIE, 4008, 1144
Leahy, J. P. 1991, in Beams and Jets in Astrophysics, ed. P. A. Hughes (Cambridge: Cambridge Univ. Press), 100
Marconi, A., Axon, D. J., Macchetto, F. D., Cappetti, A., Sparks, W. B., & Crane, P. 1997, MNRAS, 289, L21
Mason, R. E., Geballe, T. R., Packham, C., Levenson, N. A., Elitzur, M., Fisher, R. S., & Perlman, E. 2006, ApJ, 640, 612
Nagar, N. M., Falcke, H., Wilson, A. S., & Ho, L. C. 2000, ApJ, 542, 186
Ogle, P., Whysong, D., & Antonucci, R. 2006, ApJ, 647, 161
Perlman, E. S., Biretta, J. A., Sparks, W. B., Macchetto, F. D., & Leahy, J. P. 2001a, ApJ, 551, 206 (P01a)
Perlman, E. S., Sparks, W. B., Radomski, J., Packham, C., Fisher, R. S., Piña, R., & Biretta, J. A. 2001b, ApJ, 561, L51 (P01b)
Perlman, E. S., & Wilson, A. S. 2005, ApJ, 627, 140
Perlman, E. S., et al. 2003, ApJ, 599, L65
Pian, E., et al. 1998, ApJ, 492, L17
Radomski, J., et al. 2007, ApJ, submitted
Reynolds, C. S., di Matteo, T., Fabian, A. C., Hwang, U., & Canizares, C. R. 1996, MNRAS, 283, L111
Rieke, G. H., et al. 2004, ApJS, 154, 25
Risaliti, G., & Elvis, M. 2004, in Supermassive Black Holes in the Distant Universe, ed. A. J. Barger (Dordrecht: Kluwer), 187
Roche, P., Aitken, D. K., Smith, C. H., & Ward, M. H. 1991, MNRAS, 248, 606
Roche, P. F., Whitmore, B., Aitken, D. K., & Phillips, M. M. 1984, MNRAS, 207, 35
Sako, S., et al. 2003, PASP, 115, 1407
Shi, Y., Rieke, G. H., Hines, D. C., Gordon, K. D., & Egami, E. 2007, ApJ, 655, 781
Shi, Y., et al. 2006, ApJ, 653, 127
Siebenmorgen, R., et al. 2005, A&A, 436, L5
Sparks, W. B., Ford, H. C., & Kinney, A. L. 1993, ApJ, 413, 531
Sparks, W. B., Fraix-Burnet, D., Macchetto, F., & Owen, F. N. 1992, Nature, 355, 804
Stiavelli, M., Biretta, J., Möller, P., & Zeilinger, W. W. 1992, Nature, 355, 802
Sturm, E., Lutz, D., Verma, A., Netzer, H., Sternberg, A., Moorwood, A. F. M., Oliva, E., & Genzel, R. 2002, A&A, 393, 821
Sturm, E., et al. 2005, ApJ, 629, L21
Tan, J. C., & Blackman, E. G. 2005, MNRAS, 362, 983
Tokunaga, A. 1984, AJ, 89, 172
Tsvetanov, Z. I., et al. 1998, ApJ, 493, L83
Whysong, D., & Antonucci, R. R. J. 2004, ApJ, 602, 116
Willner, S. P., Elvis, M., Fabbiano, G., Lawrence, A., & Ward, M. J. 1985, ApJ, 299, 443